Interference Effect from Buried Interfaces Investigated by Angular-Dependent Infrared–Visible Sum Frequency Generation Technique

ARTICLE *in* THE JOURNAL OF PHYSICAL CHEMISTRY C · MARCH 2011

Impact Factor: 4.77 · DOI: 10.1021/jp2000249

3 AUTHORS, INCLUDING:

Ali Dhinojwala
University of Akron
175 PUBLICATIONS **2,866** CITATIONS

SEE PROFILE

THE JOURNAL OF PHYSICAL CHEMISTRY C

ARTICLE

pubs.acs.org/JPCC

Interference Effect from Buried Interfaces Investigated by Angular-Dependent Infrared−Visible Sum Frequency Generation Technique

Guifeng Li,[†] Ali Dhinojwala,[*,†] and Mohsen S. Yeganeh[*,‡]

[†]Department of Polymer Science, The University of Akron, Akron, Ohio 44325, United States

[‡]Corporate Strategic Research, ExxonMobil Research and Engineering Company, Annandale, New Jersey 08801, United States

Supporting Information

ABSTRACT: Infrared-visible sum frequency generation spectroscopy (SFG) in conjunction with total internal reflection geometry (TIR) has been demonstrated as a powerful technique to study buried polymer interfaces. We have developed a theoretical model using linear and nonlinear boundary conditions to calculate the SFG signals as a function of incident angles and thickness of the polymer films. The validity of this model is tested using a polystyrene film (PS) coated on a sapphire prism. This PS film is exposed to heneicosane ($C_{21}H_{44}$) above and below its melting temperature. At temperatures greater than T_m, the SFG contributions from both interfaces (PS/sapphire and alkane/PS) are comparable and we observe strong interference effects. At temperatures below T_m, the SFG signals are dominated by the methyl signals of all-trans heneicosane molecules at the alkane/PS interface. The theoretical model is able to accurately capture the angle and thickness dependence of the SFG signal and provides a valuable tool to accurately determine the interference effects in multilayer samples using SFG in total internal reflection geometry. The model also provides physical parameters (i.e., film thickness, incident angle and substrate index of refraction) needed to suppress or enhance SFG signals generated at a particular interface.

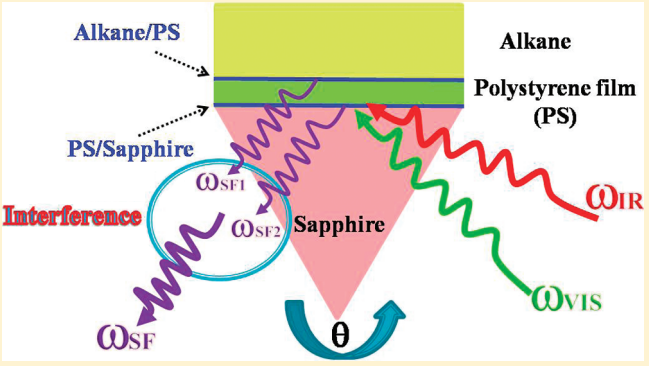

INTRODUCTION

Interfaces are ubiquitous in physical, chemical, and biological processes.[1,2] Molecular characterization of buried interfaces has been difficult because the traditional spectroscopic techniques such as infrared, Raman, and NMR are either not suitable or not sensitive enough to study nanometer-thin interfacial layers buried deep inside the bulk materials. In the last two decades there has been considerable progress in the development of surface-sensitive infrared-visible sum frequency generation spectroscopy (SFG) to study a variety of organic and inorganic interfaces.[3−9] Using the dipole approximation, this second-order nonlinear process is forbidden in the bulk of isotropic materials and is only allowed at surfaces and interfaces where the inversion symmetry is broken. The intrinsic interface sensitivity of SFG allows investigations of buried interfaces that are not easily accessible by other techniques.[4,10] The SFG signals are enhanced when the scanning IR wavelengths overlap with the molecular stretching vibrations that are infrared and Raman active. The SFG intensity and peak position can be used to determine the orientation and chemical composition of the surface groups.

In the past decade, SFG has been extensively used to probe interfaces in polymer films[9,11] in contact with air,[9,11] liquid,[12−16] other polymers,[17−19] or inorganic solids.[11,20] By combining SFG with total internal reflection geometry (TIR), it is possible to isolate the contribution of individual interfaces in a multilayer geometry.[11,14,17] The use of this approach was demonstrated with a thin polystyrene (PS) film spin coated on a sapphire prism.[11] The SFG signals were monitored as a function of incident angle. The SFG signals were enhanced when the incident angles were near the critical angles for total internal reflection for PS/sapphire or PS/air interfaces. By taking advantage of the enhancement in SFG signals at critical angles, we determined the molecular orientation and composition at these two interfaces. This technique has now been applied to study a variety of different polymers and systems.[11,17,21]

Even though the combination of SFG and TIR is a powerful tool to probe buried interfaces, the application of this technique to study buried interfaces of materials that are similar in refractive indices has been complicated. The interference of the signal generated from multiple interfaces makes it difficult to uniquely separate the contribution from individual interfaces. Although several groups have developed models for polymer/metal coatings[20,22,23] and monolayer/dielectric film/Au layers,[24,25] the model for angular dependence of SFG-TIR for polymer films

Received: January 2, 2011
Revised: February 25, 2011
Published: March 31, 2011

has not been developed. In this paper, we have developed a theoretical model using linear and nonlinear boundary conditions. This model predicts the angular and thickness dependence of SFG signals in SSP polarization. We have developed the model for SSP polarization because this is the most common polarization used to quantify the orientation of molecules at the interface. We have tested this model with a PS film spin coated on a sapphire prism and in contact with heneicosane at temperatures higher and lower than heneicosane melting temperature. This model can be used to separate the contribution from multiple interfaces encountered in many areas such as adhesion, friction, and wetting. In addition, this model provides guidance on the film thickness for further enhancement of the SFG spectroscopy of buried interfaces.

EXPERIMENTAL SECTION

Sample Preparation. Polystyrene (PS, M_w = 382,100, T_g = 100 °C, Aldrich) and heneicosane ($C_{21}H_{44}$, 98%, T_m = 39 °C, Aldrich) were used as received. A sapphire prism was cleaned in an ultrasonic bath of toluene for 2 h; rinsed with acetone, ethanol, and heptane; dried with N_2; and finally cleaned in the plasma cleaner. A PS thin film (500 nm) was spin-coated on a 60° sapphire prism (1500 rpm) from 5 wt % PS/toluene solution. The PS film was annealed in a vacuum oven at 120 °C for about 10 h.

For the PS/alkane experiments, heneicosane was filled in a syringe and preheated to 50 °C for 3−5 min before transferring to a preheated stainless steel SFG cell for measurements. The SFG sample was maintained at 60 °C to prevent freezing of heneicosane during filling of the sample cell. The temperature of the sample cell filled with heneicosane was cooled to room temperature at a rate of 0.5 °C/min to eliminate the formation of air bubble. Because the sample cell is completely filled with alkane, we eliminated the alkane/air interface.

SFG System. A nanosecond SFG system was used in the present experiments.[26] The details of the system are given elsewhere. Briefly, the sum frequency generation signal was generated by overlapping a 532 nm visible laser beam with a tunable infrared laser beam. The tunable infrared laser beam was generated using stimulated Raman scattering in a multipass hydrogen cell. The difference of incident angle of visible and IR laser beam was less than 0.5°. SFG signals were collected by a PMT detector. In the present studies, SFG spectra were recorded at different incident angles in SSP polarization configurations (s-SF, s-v, and p-IR). The incident angles reported in this paper are with respect to the surface normal of sapphire prism. The values of refractive indices, thickness of PS films, and Aq values are provided in the Supporting Information.

RESULTS AND DISCUSSION

Theoretical Model. In this section we will develop the linear and nonlinear boundary conditions for total internal reflection geometry. The predictions from this model will be compared with experimental results presented in the next section. Figure 1 shows the schematic of the electromagnetic field propagating in the sample in S-polarization where the symbols "0", "1", "a", and "b" represents air, sapphire prism, PS, and heneicosane. The symbols "a′ " and "b′ " represent PS/sapphire and PS/heneicosane interfaces, respectively. Within the dipole approximation, the second-order polarization generated at the interfacial layer j (j = a′ and b′) as[10]

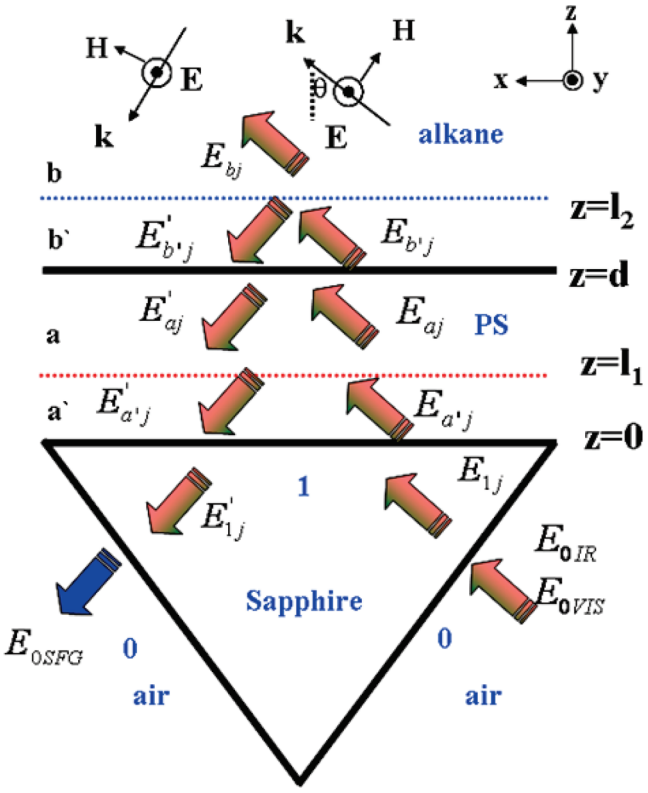

Figure 1. Schematic of electromagnetic field in the sapphire/polystyrene (PS)/alkane system under s-polarization. Incident electric field (j = SFG, VIS, and IR) in medium (i = 1, a, a′, b′, and b) are expressed by E_{ij}. Reflected electric field (j = SFG, VIS, and IR) in medium (i = 1, a, a′, b′, and b) are expressed by E'_{ij}. SFG contributions are from interfacial layer a′ and b′. The symbols 1, a, and b are for sapphire, PS, and alkane, respectively. a′ is interfacial layer between sapphire and PS and b′ is interfacial layer between PS and alkane.

$$P_j^{(2)} = \chi_j^{(2)} E_{j,v} E_{j,IR} \qquad (j = a' \text{ and } b') \tag{1}$$

where $\chi_j^{(2)}$ is the second-order susceptibility tensor of the interfacial layer j. $E_{j,v}$ and $E_{j,IR}$ are the visible and infrared electric fields in the interfacial layer j. The second-order polarization, $P^{(2)}$, produces a SFG electric field at the interface which then propagates through the system reaching the medium "1" (prism). The SFG electric field in medium "1" can be written as follows:

$$E_{1,SFG} = \sum_{j}^{j=a',b'} G_{j,SFG} P_j^{(2)} = \sum_{j}^{j=a',b'} G_{j,SFG} \chi_j^{(2)} E_{j,v} E_{j,IR} \tag{2}$$

Here, $G_{j,SFG}$ is a SF Fresnel coefficient which describes the propagation of the induced nonlinear field (SFG) from the interfacial layer j to medium "1". The visible and infrared electric fields in the interfacial layer "j" ($E_{j,v}$ and $E_{j,IR}$) are related to the two incoming electric fields ($E_{1,v}$ and $E_{1,IR}$) in medium "1" by a linear Fresnel coefficient ($L_{j,v}$ and $L_{j,IR}$) as follows:

$$E_{j,v} = L_{j,v} E_{1,v} \tag{3}$$

$$E_{j,IR} = L_{j,IR} E_{1,IR} \tag{4}$$

The electric fields in "1" are related to electric fields in "0" using the transmission coefficients. Thus one can express the

SFG electric field in medium "0" as

$$E_{0,\mathrm{SFG}} = \sum_{\mathrm{j}}^{\mathrm{j=a',b'}} G_{\mathrm{j,SFG}} L_{\mathrm{j,v}} L_{\mathrm{j,IR}} t_{01,\mathrm{v}} t_{01,\mathrm{IR}} t^{s}_{10} \chi^{(2)}_{\mathrm{j}} E_{0,\mathrm{v}} E_{0,\mathrm{IR}} \quad (5)$$

The SFG intensity ($I_{0,\mathrm{SFG}}$) propagating in the medium "0" is thus

$$I_{0,\mathrm{SFG}} = \frac{c}{8\pi} \left| \sum_{\mathrm{j}}^{\mathrm{j=a',b'}} G_{\mathrm{j,SFG}} L_{\mathrm{j,v}} L_{\mathrm{j,IR}} t_{01,\mathrm{v}} t_{01,\mathrm{IR}} t^{s}_{10} \chi^{(2)}_{\mathrm{j}} \right|^2 I_{0,\mathrm{v}} I_{0,\mathrm{IR}} \quad (6)$$

Here, c is the speed of light in a vacuum. $I_{0,\mathrm{v}}$ and $I_{0,\mathrm{IR}}$ are the intensity of the visible and IR light, in medium "0", respectively. In this paper we are only concerned with the s-polarized SFG signal generated with an s-polarized visible and a p-polarized IR beam. In the next section, we provide the details for determining $L_{\mathrm{j,v}}$ (s-polarized), $L_{\mathrm{j,IR}}$ (p-polarized), and $G_{\mathrm{j,SFG}}$ (s-polarized) Fresnel coefficients.

Calculation of s-Polarized Linear Fresnel Coefficient. Using Figure 1, the linear boundary conditions at the polymer/sapphire interface are given by the following set of equations:

$$\Delta E^{y}_{1,\mathrm{a'}} = (E_{\mathrm{a',v}} + E'_{\mathrm{a,v}}) - (E_{1,\mathrm{v}} + E'_{1,\mathrm{v}}) = 0 \quad (7)$$

$$\Delta H^{x}_{1,\mathrm{a'}} = (-n^{\mathrm{v}}_{\mathrm{a'}} E_{\mathrm{a',v}} \cos\theta^{\mathrm{v}}_{\mathrm{a'}} + n^{\mathrm{v}}_{\mathrm{a'}} E'_{\mathrm{a',v}} \cos\theta^{\mathrm{v}}_{\mathrm{a'}}) - (-n^{\mathrm{v}}_{1} E_{1,\mathrm{v}} \cos\theta^{\mathrm{v}}_{1} + n^{\mathrm{v}}_{1} E'_{1,\mathrm{v}} \cos\theta^{\mathrm{v}}_{1}) = 0 \quad (8)$$

$$\Delta E^{y}_{\mathrm{a',a}} = (E_{\mathrm{a,v}} e^{ik^{\mathrm{v}}_{\mathrm{az}} l_1} + E'_{\mathrm{a,v}} e^{-ik^{\mathrm{v}}_{\mathrm{az}} l_1}) - (E_{\mathrm{a',v}} e^{ik^{\mathrm{v}}_{\mathrm{a'z}} l_1} + E'_{\mathrm{a',v}} e^{-ik^{\mathrm{v}}_{\mathrm{a'z}} l_1}) = 0 \quad (9)$$

$$\Delta H^{x}_{\mathrm{a',a}} = (n^{\mathrm{v}}_{\mathrm{a}} E'_{\mathrm{a,v}} e^{-ik^{\mathrm{v}}_{\mathrm{az}} l_1} \cos\theta^{\mathrm{v}}_{\mathrm{a}} - n^{\mathrm{v}}_{\mathrm{a}} E_{\mathrm{a,v}} e^{ik^{\mathrm{v}}_{\mathrm{az}} l_1} \cos\theta^{\mathrm{v}}_{\mathrm{a}}) - (n^{\mathrm{v}}_{\mathrm{a'}} E'_{\mathrm{a',v}} e^{-ik^{\mathrm{v}}_{\mathrm{a'z}} l_1} \cos\theta^{\mathrm{v}}_{\mathrm{a'}} - n^{\mathrm{v}}_{\mathrm{a'}} E_{\mathrm{a',v}} e^{ik^{\mathrm{v}}_{\mathrm{a'z}} l_1} \cos\theta^{\mathrm{v}}_{\mathrm{a'}}) = 0 \quad (10)$$

The linear boundary conditions at the polymer/alkane interfacial layer are as follows:

$$\Delta E^{y}_{\mathrm{a,b'}} = (E_{\mathrm{b',v}} e^{ik^{\mathrm{v}}_{\mathrm{b'z}} d} + E'_{\mathrm{b',v}} e^{-ik^{\mathrm{v}}_{\mathrm{b'z}} d}) - (E_{\mathrm{a,v}} e^{ik^{\mathrm{v}}_{\mathrm{bz}} d} + E'_{\mathrm{a,v}} e^{-ik^{\mathrm{v}}_{\mathrm{bz}} d}) = 0 \quad (11)$$

$$\Delta H^{x}_{\mathrm{a,b'}} = (n^{\mathrm{v}}_{\mathrm{b'}} E'_{\mathrm{b',v}} e^{-ik^{\mathrm{v}}_{\mathrm{b'z}} d} \cos\theta^{\mathrm{v}}_{\mathrm{b'}} - n^{\mathrm{v}}_{\mathrm{b'}} E_{\mathrm{b',v}} e^{ik^{\mathrm{v}}_{\mathrm{b'z}} d} \cos\theta^{\mathrm{v}}_{\mathrm{b'}}) - (n^{\mathrm{v}}_{\mathrm{a}} E'_{\mathrm{a,v}} e^{-ik^{\mathrm{v}}_{\mathrm{az}} d} \cos\theta^{\mathrm{v}}_{\mathrm{a}} - n^{\mathrm{v}}_{\mathrm{a}} E_{\mathrm{a,v}} e^{ik^{\mathrm{v}}_{\mathrm{az}} d} \cos\theta^{\mathrm{v}}_{\mathrm{a}}) = 0 \quad (12)$$

$$\Delta E^{y}_{\mathrm{b',b}} = E_{\mathrm{b,v}} e^{ik^{\mathrm{v}}_{\mathrm{bz}} l_2} - (E_{\mathrm{b',v}} e^{ik^{\mathrm{v}}_{\mathrm{b'z}} l_2} + E'_{\mathrm{b',v}} e^{-ik^{\mathrm{v}}_{\mathrm{b'z}} l_2}) = 0 \quad (13)$$

$$\Delta H^{x}_{\mathrm{b',b}} = -n^{\mathrm{v}}_{\mathrm{b}} E_{\mathrm{b,v}} e^{ik^{\mathrm{v}}_{\mathrm{bz}} l_2} \cos\theta^{\mathrm{v}}_{\mathrm{b}} - (-n^{\mathrm{v}}_{\mathrm{b'}} E_{\mathrm{b',v}} e^{ik^{\mathrm{v}}_{\mathrm{b'z}} l_2} \cos\theta^{\mathrm{v}}_{\mathrm{b'}} + n^{\mathrm{v}}_{\mathrm{b'}} E'_{\mathrm{b',v}} e^{-ik^{\mathrm{v}}_{\mathrm{b'z}} l_2} \cos\theta^{\mathrm{v}}_{\mathrm{b'}}) = 0 \quad (14)$$

From the above equations and setting ($l_1 \rightarrow 0$ and $l_2 \rightarrow d$) the linear Fresnel coefficients for an s-polarized visible beam for both interfacial layers are as

$$L^{y}_{\mathrm{a',v}} = \frac{E_{\mathrm{a',v}}}{E_{1,\mathrm{v}}} + \frac{E'_{\mathrm{a',v}}}{E_{1,\mathrm{v}}} = \frac{2n^{\mathrm{v}}_{1} \cos\theta^{\mathrm{v}}_{1} [n^{\mathrm{v}}_{\mathrm{a}} \cos\theta^{\mathrm{v}}_{\mathrm{a}} (1 + e^{2ik^{\mathrm{v}}_{\mathrm{az}} d}) + n^{\mathrm{v}}_{\mathrm{b}} \cos\theta^{\mathrm{v}}_{\mathrm{b}} (1 - e^{2ik^{\mathrm{v}}_{\mathrm{az}} d})]}{n^{\mathrm{v}}_{1} \cos\theta^{\mathrm{v}}_{1} [n^{\mathrm{v}}_{\mathrm{a}} \cos\theta^{\mathrm{v}}_{\mathrm{a}} (1 + e^{2ik^{\mathrm{v}}_{\mathrm{az}} d}) + n^{\mathrm{v}}_{\mathrm{b}} \cos\theta^{\mathrm{v}}_{\mathrm{b}} (1 - e^{2ik^{\mathrm{v}}_{\mathrm{az}} d})] + n^{\mathrm{v}}_{\mathrm{a}} \cos\theta^{\mathrm{v}}_{\mathrm{a}} [n^{\mathrm{v}}_{\mathrm{a}} \cos\theta^{\mathrm{v}}_{\mathrm{a}} (1 - e^{2ik^{\mathrm{v}}_{\mathrm{az}} d}) + n^{\mathrm{v}}_{\mathrm{b}} \cos\theta^{\mathrm{v}}_{\mathrm{b}} (1 + e^{2ik^{\mathrm{v}}_{\mathrm{az}} d})]} \quad (15)$$

$$L^{y}_{\mathrm{b',v}} = \frac{E_{\mathrm{b',v}}}{E_{1,v}} e^{ik^{\mathrm{v}}_{\mathrm{b'z}} d} + \frac{E'_{\mathrm{b',v}}}{E_{1,\mathrm{v}}} e^{-ik^{\mathrm{v}}_{\mathrm{b'z}} d} = \frac{4n^{\mathrm{v}}_{1} n^{\mathrm{v}}_{\mathrm{a}} \cos\theta^{\mathrm{v}}_{1} \cos\theta^{\mathrm{v}}_{\mathrm{a}} e^{ik^{\mathrm{v}}_{\mathrm{az}} d}}{n^{\mathrm{v}}_{1} \cos\theta^{\mathrm{v}}_{1} [n^{\mathrm{v}}_{\mathrm{a}} \cos\theta^{\mathrm{v}}_{\mathrm{a}} (1 + e^{2ik^{\mathrm{v}}_{\mathrm{az}} d}) + n^{\mathrm{v}}_{\mathrm{b}} \cos\theta^{\mathrm{v}}_{\mathrm{b}} (1 - e^{2ik^{\mathrm{v}}_{\mathrm{az}} d})] + n^{\mathrm{v}}_{\mathrm{a}} \cos\theta^{\mathrm{v}}_{\mathrm{a}} [n^{\mathrm{v}}_{\mathrm{a}} \cos\theta^{\mathrm{v}}_{\mathrm{a}} (1 - e^{2ik^{\mathrm{v}}_{\mathrm{az}} d}) + n^{\mathrm{v}}_{\mathrm{b}} \cos\theta^{\mathrm{v}}_{\mathrm{b}} (1 + e^{2ik^{\mathrm{v}}_{\mathrm{az}} d})]} \quad (16)$$

In these equations $E_{\mathrm{i,v}}$ and $E'_{\mathrm{i,v}}$ are incident and reflected electric fields in medium "i" where i can be a', a, b', or b. Similarly, $n^{\mathrm{v}}_{\mathrm{i}}$ is the refractive index, $\theta^{\mathrm{v}}_{\mathrm{i}}$ is the incident angle, and $k^{\mathrm{v}}_{\mathrm{iz}}$ is the z-component of the wavevector of the visible beam in medium "i" where i can be a', a, b', or b.

Calculation of p-Polarized Linear Fresnel Coefficient. In the case of electromagnetic field propagating in p-polarization we can interchange the E and H fields in Figure 1. The linear boundary conditions for p-polarized light at the sapphire/polymer interface are

$$\Delta E^{x}_{1,\mathrm{a'}} = (E_{\mathrm{a',IR}} \cos\theta^{\mathrm{i}}_{\mathrm{a'}} + E'_{\mathrm{a',IR}} \cos\theta^{\mathrm{i}}_{\mathrm{a'}}) - (E_{1,\mathrm{IR}} \cos\theta^{\mathrm{i}}_{1} + E'_{1,\mathrm{IR}} \cos\theta^{\mathrm{i}}_{1}) = 0 \quad (17)$$

$$\Delta H^{y}_{1,\mathrm{a'}} = (n^{\mathrm{i}}_{\mathrm{a'}} E_{\mathrm{a',IR}} - n^{\mathrm{i}}_{\mathrm{a'}} E'_{\mathrm{a',IR}}) - (n^{\mathrm{i}}_{1} E_{1,\mathrm{IR}} - n^{\mathrm{i}}_{1} E'_{1,\mathrm{IR}}) = 0 \quad (18)$$

$$\Delta E^{x}_{\mathrm{a',a}} = (E'_{\mathrm{a,IR}} e^{-ik^{\mathrm{i}}_{\mathrm{az}} l_1} \cos\theta^{\mathrm{i}}_{\mathrm{a}} + E_{\mathrm{a,IR}} e^{ik^{\mathrm{i}}_{\mathrm{az}} l_1} \cos\theta^{\mathrm{i}}_{\mathrm{a}}) - (E'_{\mathrm{a',IR}} e^{-ik^{\mathrm{i}}_{\mathrm{a'z}} l_1} \cos\theta^{\mathrm{i}}_{\mathrm{a'}} + E_{\mathrm{a',IR}} e^{ik^{\mathrm{i}}_{\mathrm{a'z}} l_1} \cos\theta^{\mathrm{i}}_{\mathrm{a'}}) = 0 \quad (19)$$

$$\Delta H^{y}_{\mathrm{a',a}} = (n^{\mathrm{i}}_{\mathrm{a}} E_{\mathrm{a,IR}} e^{ik^{\mathrm{i}}_{\mathrm{az}} l_1} - n^{\mathrm{i}}_{\mathrm{a}} E'_{\mathrm{a,IR}} e^{-ik^{\mathrm{i}}_{\mathrm{az}} l_1}) - (n^{\mathrm{i}}_{\mathrm{a'}} E_{\mathrm{a',IR}} e^{ik^{\mathrm{i}}_{\mathrm{a'z}} l_1} - n^{\mathrm{i}}_{\mathrm{a'}} E'_{\mathrm{a',IR}} e^{-ik^{\mathrm{i}}_{\mathrm{a'z}} l_1}) = 0 \quad (20)$$

The linear boundary conditions at the polymer/alkane interfacial layer are as follows:

$$\Delta E^{x}_{\mathrm{a,b'}} = (E'_{\mathrm{b',IR}} e^{-ik^{\mathrm{i}}_{\mathrm{b'z}} d} \cos\theta^{\mathrm{i}}_{\mathrm{b'}} + E_{\mathrm{b',IR}} e^{ik^{\mathrm{i}}_{\mathrm{b'z}} d} \cos\theta^{\mathrm{i}}_{\mathrm{b'}}) - (E'_{\mathrm{a,IR}} e^{-ik^{\mathrm{i}}_{\mathrm{az}} d} \cos\theta^{\mathrm{i}}_{\mathrm{a}} + E_{\mathrm{a,IR}} e^{ik^{\mathrm{i}}_{\mathrm{az}} d} \cos\theta^{\mathrm{i}}_{\mathrm{a}}) = 0 \quad (21)$$

$$\Delta H^{y}_{\mathrm{a,b'}} = (n^{\mathrm{i}}_{\mathrm{b'}} E_{\mathrm{b',IR}} e^{ik^{\mathrm{i}}_{\mathrm{b'z}} d} - n^{\mathrm{i}}_{\mathrm{b'}} E'_{\mathrm{b',IR}} e^{-ik^{\mathrm{i}}_{\mathrm{b'z}} d})$$

dx.doi.org/10.1021/jp2000249 |J. Phys. Chem. C 2011, 115, 7554–7561

$$-(n_{a}^{i}E_{a,IR}e^{ik_{az}^{i}d}-n_{a}^{i}E_{a,IR}^{'}e^{-ik_{az}^{i}d})=0 \quad (22)$$

$$\Delta E_{b',b}^{x}=E_{b,IR}e^{ik_{bz}^{i}l_2}\cos\theta_{b}^{i}-(E_{b',IR}^{'}e^{-ik_{b'z}^{i}l_2}\cos\theta_{b'}^{i}+E_{b',IR}e^{ik_{b'z}^{i}l_2}\cos\theta_{b'}^{i})=0 \quad (23)$$

$$\Delta H_{b',b}^{y}=n_{b}^{i}E_{b,IR}e^{ik_{bz}^{i}l_2}-(n_{b'}^{i}E_{b',IR}e^{ik_{b'z}^{i}l_2}-n_{b'}^{i}E_{b',IR}^{'}e^{-ik_{b'z}^{i}l_2})=0 \quad (24)$$

From the above equations and setting ($l_1 \rightarrow 0$ and $l_2 \rightarrow d$) the linear Fresnel coefficients for p-polarized infrared beam for both interfacial layers are as follows:

$$L_{a',IR}^{z}=\left(\frac{E_{a',IR}}{E_{1,IR}}-\frac{E_{a',IR}^{'}}{E_{1,IR}}\right)\frac{n_{1}^{i}}{n_{a'}^{i}}=\frac{2(n_{1}^{i})^{2}n_{a}^{i}\cos\theta_{1}^{i}[n_{b}^{i}\cos\theta_{a}^{i}(1+e^{2ik_{az}^{i}d})+n_{a}^{i}\cos\theta_{b}^{i}(1-e^{2ik_{az}^{i}d})]}{(n_{a'}^{i})^{2}[\cos\theta_{1}^{i}\cos\theta_{b}^{i}(n_{a}^{i})^{2}(1-e^{2ik_{az}^{i}d})+n_{1}^{i}n_{b}^{i}\cos^{2}\theta_{a}^{i}(1-e^{2ik_{az}^{i}d})]+n_{a}^{i}\cos\theta_{a}^{i}[(n_{b}^{i}\cos\theta_{1}^{i}+n_{1}^{i}\cos\theta_{b}^{i})(1+e^{2ik_{az}^{i}d})]} \quad (25)$$

$$L_{b',IR}^{z}=\left(\frac{E_{b',i}}{E_{1,i}}e^{ik_{b'z}^{i}d}-\frac{E_{b',i}^{'}}{E_{1,i}}e^{-ik_{b'z}^{i}d}\right)\frac{n_{1}^{i}}{n_{b'}^{i}}=\frac{4(n_{1}^{i})^{2}n_{a}^{i}n_{b}^{i}\cos\theta_{1}^{i}\cos\theta_{a}^{i}e^{ik_{az}^{i}d}}{(n_{b'}^{i})^{2}[\cos\theta_{1}^{i}\cos\theta_{b}^{i}(n_{a}^{i})^{2}(1-e^{2ik_{az}^{i}d})+n_{1}^{i}n_{b}^{i}\cos^{2}\theta_{a}^{i}(1-e^{2ik_{az}^{i}d})]+n_{a}^{i}\cos\theta_{a}^{i}[(n_{b}^{i}\cos\theta_{1}^{i}+n_{1}^{i}\cos\theta_{b}^{i})(1+e^{2ik_{az}^{i}d})]} \quad (26)$$

In these equations $E_{i,IR}$ and $E'_{i,IR}$ are incident and reflected electric fields, n_i is the refractive index, θ_i is the incident angle, and k_{iz} is the z-component of the wavevector of the IR beam in medium "i" where i can be a′, a, b′, or b.

Calculation of s-Polarized SF Fresnel Coefficient. The general form of the nonlinear boundary conditions for an s-polarized SFG beam are[27]

$$\Delta E_{y}=-\frac{4\pi}{n_{b'}^{2}}\frac{\partial P_{z}^{s}}{\partial y}=0 \quad (27)$$

$$\Delta H_{x}=-\frac{4\pi i\omega}{c}P_{y}^{s} \quad (28)$$

Using Figure 1 and $l_1 \rightarrow 0$, the above nonlinear boundary conditions for the sapphire/polymer interface become

$$\Delta E_{1a}^{y}=(E_{a,SFG}+E_{a,SFG}^{'})-E_{1,SFG}^{'}=0 \quad (29)$$

$$\Delta H_{1a}^{x}=(n_{a}^{s}E_{a,SFG}^{'}\cos\theta_{a}^{s}-n_{a}^{s}E_{a,SFG}\cos\theta_{a}^{s})-n_{1}^{s}E_{1,SFG}^{'}\cos\theta_{1}^{s}=-\frac{4\pi i\omega}{c}P_{y1}^{s} \quad (30)$$

Similarly, with $l_2 \rightarrow d$, the boundary conditions for the polymer/alkane interface can be written as follows:

$$\Delta E_{ab}^{y}=E_{b,SFG}e^{ik_{bz}^{s}d}-(E_{a,SFG}e^{ik_{az}^{s}d}+E_{a,SFG}^{'}e^{-ik_{az}^{s}d})=0 \quad (31)$$

$$\Delta H_{ab}^{x}=(-n_{b}^{s}E_{b,SFG}e^{ik_{bz}^{s}d}\cos\theta_{b}^{s})-(n_{a}^{s}e^{-ik_{az}^{s}d}\cos\theta_{a}^{s}-n_{a}^{s}E_{a,SFG}e^{ik_{az}^{s}d}\cos\theta_{a}^{s})=-\frac{4\pi i\omega}{c}P_{y2}^{s} \quad (32)$$

Solving the above nonlinear boundary conditions yields $G_{a',SFG}^{y}$ and $G_{b',SFG}^{y}$ as follows:

$$G_{a',SFG}^{y}=\frac{E_{a',SFG}}{P_{a',SFG}^{(2)}}=\frac{4i\pi\omega}{c}\frac{n_{a}^{s}\cos\theta_{a}^{s}(1+e^{2ik_{az}^{s}d})+n_{b}^{s}\cos\theta_{b}^{s}(1-e^{2ik_{az}^{s}d})}{n_{1}^{s}\cos\theta_{1}^{s}[n_{a}^{s}\cos\theta_{a}^{s}(1+e^{2ik_{az}^{s}d})+n_{b}^{s}\cos\theta_{b}^{s}(1-e^{2ik_{az}^{s}d})]+n_{a}^{s}\cos\theta_{a}^{s}[n_{a}^{s}\cos\theta_{a}^{s}(1-e^{2ik_{az}^{s}d})+n_{b}^{s}\cos\theta_{b}^{s}(1+e^{2ik_{az}^{s}d})]} \quad (33)$$

$$G_{b',SFG}^{y}=\frac{E_{b',SFG}}{P_{b',SFG}^{(2)}}=\frac{4i\pi\omega}{c}\frac{2n_{a}^{s}\cos\theta_{a}^{s}e^{ik_{az}^{s}d}}{n_{1}^{s}\cos\theta_{1}^{s}[n_{a}^{s}\cos\theta_{a}^{s}(1+e^{2ik_{az}^{s}d})+n_{b}^{s}\cos\theta_{b}^{s}(1-e^{2ik_{az}^{s}d})]+n_{a}^{s}\cos\theta_{a}^{s}[n_{a}^{s}\cos\theta_{a}^{s}(1-e^{2ik_{az}^{s}d})+n_{b}^{s}\cos\theta_{b}^{s}(1+e^{2ik_{az}^{s}d})]} \quad (34)$$

Here, $E_{i,SFG}$ and $E'_{i,SFG}$ are incident and reflected electric fields in medium "i" where i can be a′, a, b′, or b. Similarly, n_i^s is the refractive index, θ_i^s is the incident angle, and k_{iz}^s is the z-component of the wavevector of the SFG beam in medium "i" where i can be a′, a, b′, or b.

Linear and SF Fresnel coefficients from the interfacial layer "b′" are described by Yeganeh et al.[28] and will not be reproduced here. We should note that by setting $d \rightarrow 0$ (a = b), all linear and SF Fresnel coefficients reduce to the following equations in agreement with the expressions reported by Hirose et al.[27]

dx.doi.org/10.1021/jp2000249 |J. Phys. Chem. C 2011, 115, 7554–7561

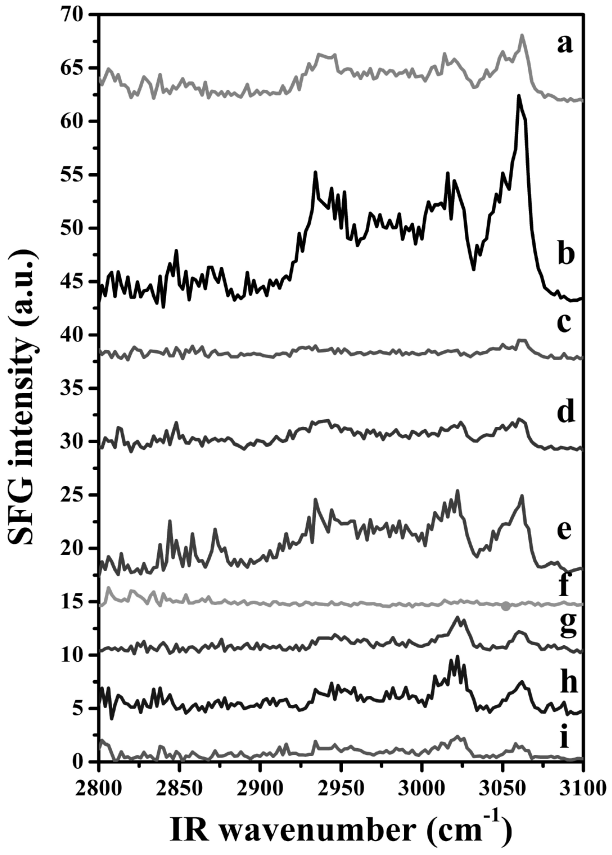

Figure 2. Angle-dependent SSP spectra of heneicosane ($C_{21}H_{44}$)/PS/sapphire system at 50 °C for (a) +10°, (b) +8°, (c) +4°, (d) −3°, (e) −4°, (f) −7°, (g) −8°, (h) −10°, and (i) −15°.

$$L^{y}_{a',v} = L^{y}_{b',v} = \frac{2n_1 \cos\theta_1}{n_b \cos\theta_b + n_1 \cos\theta_1} \quad (35)$$

$$L^{z}_{a',IR} = L^{z}_{b',IR} = \frac{2n_b \cos\theta_1}{n_1 \cos\theta_b + n_b \cos\theta_1}\left(\frac{n_1}{n_{b'}}\right)^2 \quad (36)$$

$$G^{y}_{a',SFG} = G^{y}_{b',SFG} = \frac{4i\pi\omega}{c}\frac{1}{n_1 \cos\theta_1 + n_b \cos\theta_b} \quad (37)$$

Here, n_k is the refractive index of the laser beam in medium k (k = 1, a, and b); θ_k is the angle of the laser beam in medium k (k = 1, a, and b) with respect to the surface normal.

Comparison of the Model with Experimental Results. To compare the experimental results with the theoretical model, we used the sapphire/PS/heneicosane system. In the first part of this section, we present the experimental results of PS films in contact with heneicosane above heneicosane's melting temperatures (T_m), where the signals from PS/sapphire and PS/alkane interfaces are comparable. In the second part of this section, we present the SFG spectra below where the signals from alkane molecules are much stronger than those from the PS/sapphire interface. Finally, in the third part of the section we provide theoretical insight on the effect of the PS film thickness on the angle-dependent SFG signals.

SFG Results above T_m. Figure 2 shows the SFG spectra at 50 °C at various incident angles in SSP polarization. The resonance peaks between 2850 and 3000 cm^{-1} are assigned to methylene and methyl groups of heneicosane. The resonances from 3000 to 3100 cm^{-1} are assigned to phenyl vibrations of PS. The specific assignments are provided in previous publication[14] and were confirmed using deuterated alkanes.

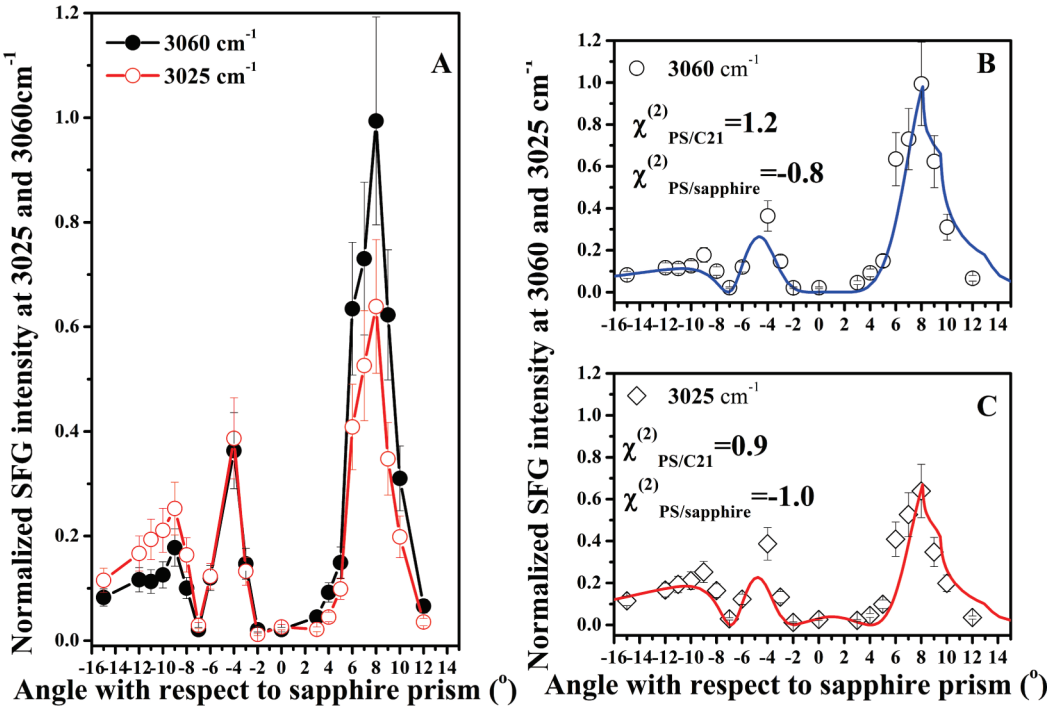

Figure 3. (A) Comparison of normalized SFG intensity at 3025 and 3060 cm^{-1} as a function of angle of the laser beam with respect to sapphire prism surface. (B) and (C) Comparison of angle-dependent experimental results (open circle dotted line for 3060 cm^{-1} (B) and open diamond dotted line for 3025 cm^{-1} (C)) and the results of the theoretical calculations are shown as solid lines.

dx.doi.org/10.1021/jp2000249 |J. Phys. Chem. C 2011, 115, 7554–7561

To understand the variation of the SFG intensity, we have plotted the SFG intensity as a function of incident angles for the phenyl peaks at 3060 and 3025 cm^{-1} in Figure 3. The SFG intensities were normalized with the peak intensity at the incident angle of 8°. As expected, the SFG intensities are higher at incident angles corresponding to the critical angles of either the PS/sapphire (near −10°) or PS/alkane (near +8°) interfaces. The solid lines depicted in Figure 3B,C, are the theoretical fit calculated using eq 6 ,which contains SFG contribution from both of the interfaces and interference effect of the signals. The fits were obtained using χ and the film thickness as the only two free parameters. The thickness of the PS film used for fitting was independently confirmed using an ellipsometer. The theoretical model accurately captures the experimental data. Interestingly, the sign of the χ for the PS/sapphire interface was the opposite of the PS/alkane interface. This is consistent with the physical picture that the orientation of the phenyl groups is in opposite directions at both the interfaces. In our previous publication[11,14,29] we have reported detailed analysis of phenyl orientation at the PS/air, PS/sapphire, and PS/alkane interfaces. The χ values obtained from the current angle-dependent measurements are similar to those reported before. However, as discussed later in this paper, the thickness used in those experiments were optimum in reducing the interference effects.

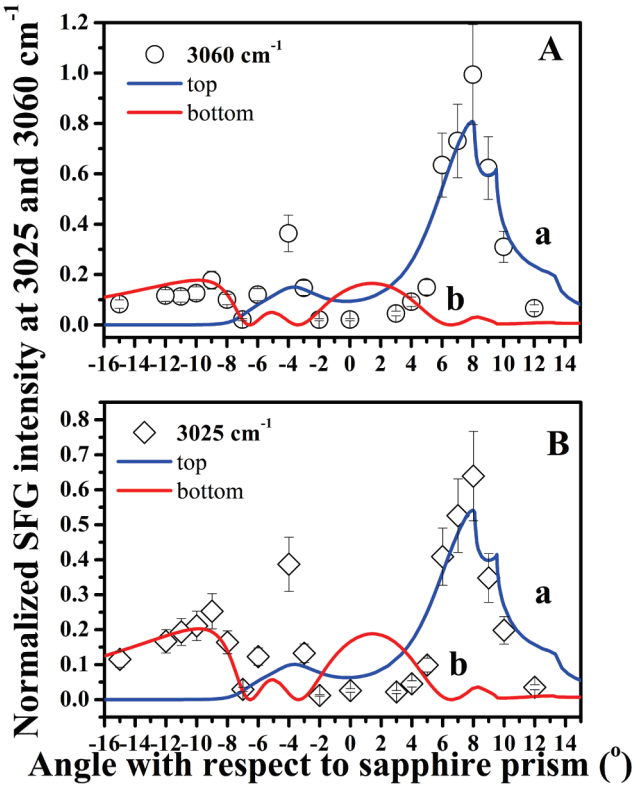

Figure 4. Comparison of angle-dependent experimental results (○ for 3060 cm^{-1} (A) and ◇ for 3025 cm^{-1} (B)) and theoretical calculations (solid line) by only considering heneicosane/PS (a) or PS/sapphire (b) interfacial contribution.

The most prominent effect of the interference of the SFG signal from both interfaces is in the region between −8° and 0°. By using a single interface model, we are unable to capture the experimental results shown in Figure 4A,B. We could only fit the region between −8° and 0° after considering the interference from both interfaces. This illustrates the importance of the complete theoretical model presented in this paper.

SFG Results Below T_m. Heneicosane undergoes a rotator-melt transition at 45 °C and rotator to crystalline transition at 35 °C. We have measured the SFG spectra in rotator and crystalline as a function of incident angles (Figure 5A,B). The dominant peaks below 3000 cm^{-1} are for the methyl symmetric and methyl-

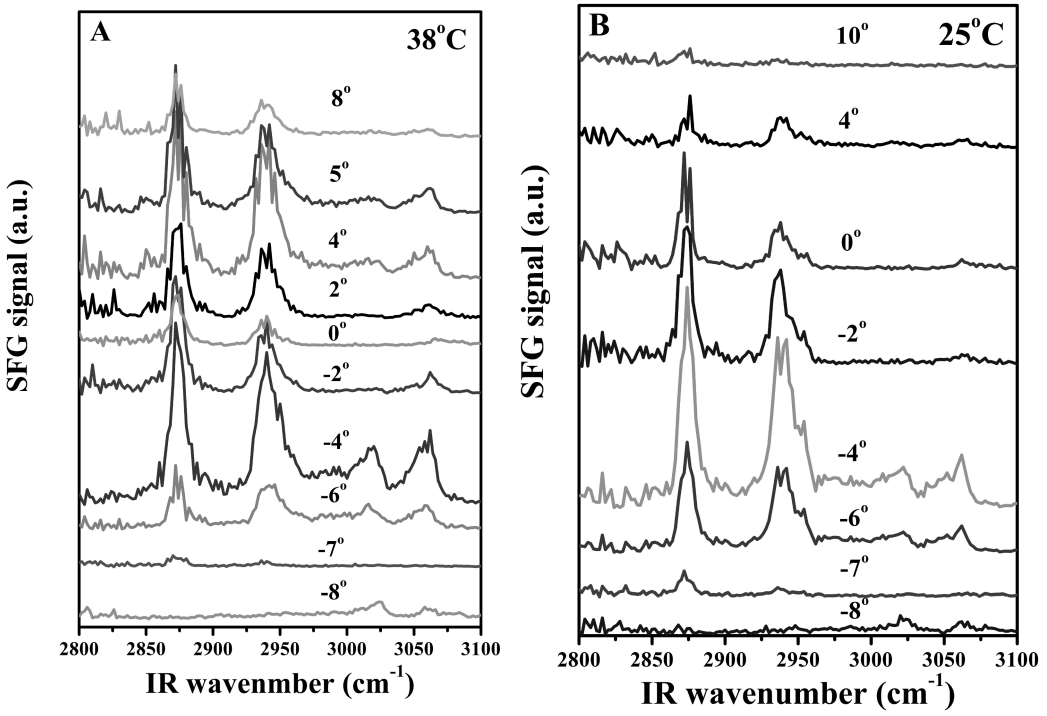

Figure 5. Angle-dependent SSP spectra of $C_{21}H_{44}$/PS/sapphire system at 38 °C (A) and 25 °C (B) at different incident angles.

dx.doi.org/10.1021/jp2000249 |J. Phys. Chem. C 2011, 115, 7554–7561

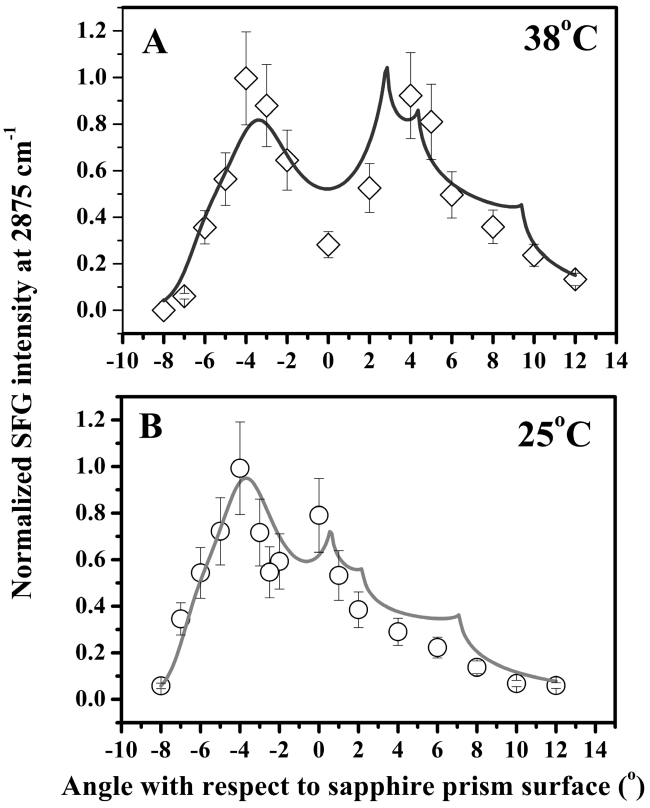

Figure 6. Comparison of angle-dependent experimental results at 2875 cm^{-1} (○ for 25 °C and ◇ for 38 °C) and theoretical calculations (solid line) by only considering nonlinear generation at the heneicosane/PS interface.

Fermi vibrations. The strong methyl signals indicate all-trans conformation of the heneicosane molecules below T_m. The normalized SFG intensity (at 2875 cm^{-1}) is plotted as a function of incident angles in Figure 6A,B. The angle-dependent behavior is extremely different in the rotator and the crystalline state. Because there is no alkane signal from the PS/sapphire interface, we have taken the χ values for the alkane peaks to be zero at the PS/sapphire interface. The angle-dependent changes observed below T_m are mainly due to the changes in the refractive indices associated with the rotator and crystalline phase.

Role of the Thickness of the Polymer Film. As it is evident from eq 6 and detailed expressions of linear and SF Fresnel coefficients, the thickness of the polymer film plays an important role in variations of the SFG signals with the angle of incidence. Figure 7A,B compares the theoretical predictions of the angle-dependent SFG signals for various film thicknesses calculated from eq 6 using experimental values of the refractive indices and χ. SFG signals from the system with film thickness of ≈500 nm show higher sensitivity to the differences between the refractive indices of the polymer film and the alkane.

The film thickness and angle of incidence can be used to enhance the SFG signals produced at a given interface, an advantage for a high signal-to-noise and selective SFG spectroscopy. The sensitivity to the film thickness is demonstrated in Figure 8A, where the SFG signal intensity as a function of film thickness at angle of incidence of 0° is displaced. Figure 8B shows the variations of contribution of each interface to the total signal intensity with thickness. These results suggest that PS film with thickness of 300 nm markedly enhances the SFG signals

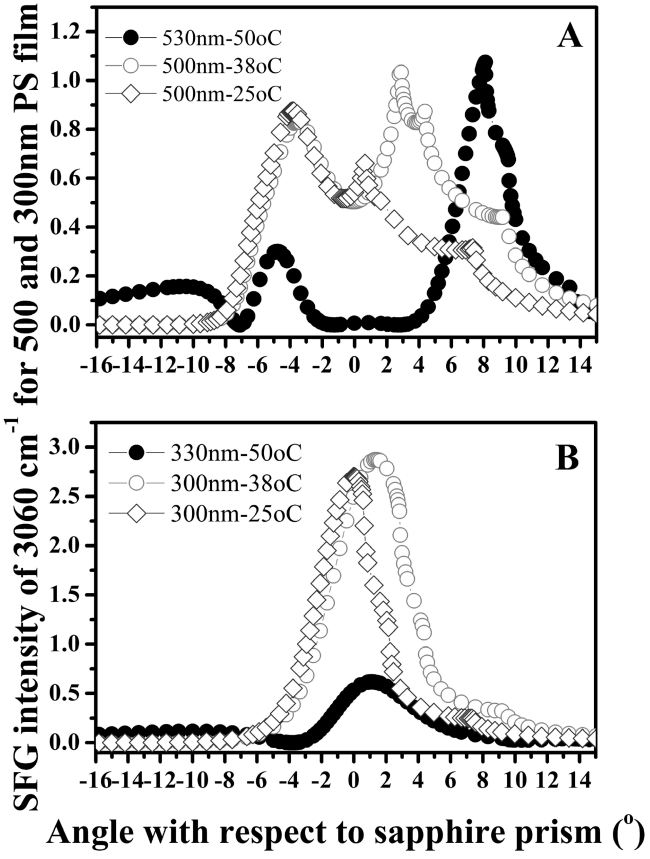

Figure 7. Calculation results of heneicosane/PS/sapphire system at 50, 38, and 25 °C when the thickness of polystyrene film is ≈500 nm (A) and ≈300 nm (B). The thickness of the film above the bulk melting temperature was taken to be slightly higher than those below T_m to account for differences in the density between the melt and crystalline state. We have used the refractive indices and χ values to calculate these results.

generated at the PS/alkane interface and significantly reduces PS/sapphire contribution to the total SFG signals, whereas the system with film thickness less than 300 nm or between 500 and 700 nm produces high signal intensities from the PS/sapphire interface with a minimum contribution from the PS/alkane interface. It should be noted that these trends are specific for the system studied here and will be different for films of different refractive indices.

SUMMARY

We have developed a theoretical model to determine the angle-dependent SFG intensity in a total internal reflection geometry. This model was tested using an example of PS film on a sapphire prism. The PS film was brought in contact with heneicosane above and below its bulk melting temperature. The angle dependence was a strong function of refractive index, thickness of the polymer film, and the interference of the SFG signals from both the interfaces (polymer/sapphire and polymer/alkane). By fitting the angle-dependence data, one could directly determine the magnitude and sign of the χ parameters. The phase information provides the direction of the orientation of the side chains. The development of this model will also aid in optimizing the experimental conditions to either enhance or reduce the effects of buried interfaces. These results also illustrate that monitoring the changes in the SFG intensities is not

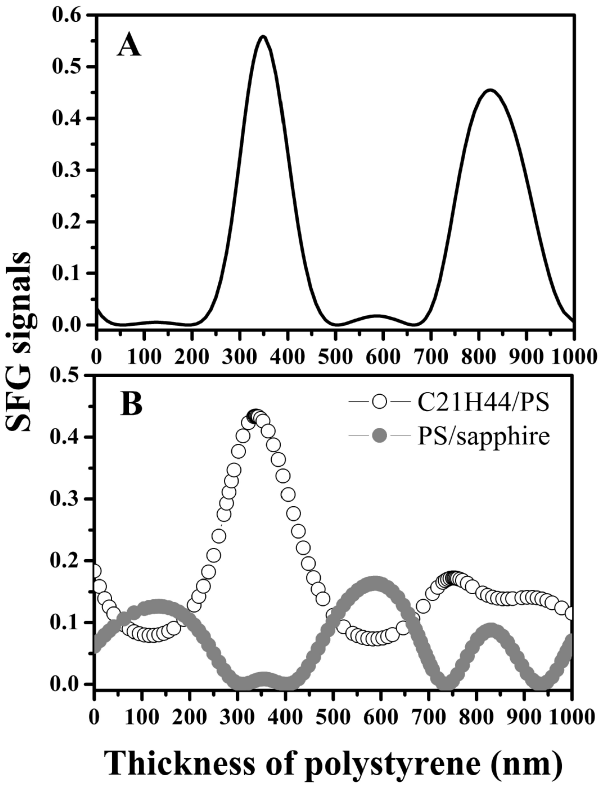

Figure 8. (A) SFG signals at 50 °C considering heneicosane/PS and PS/sapphire contributions, and (B) SFG signals considering only heneicosane/PS (○) or PS/sapphire (●) interfaces. These calculations were done at the incident angles of 0°.

sufficient to predict structural changes without accounting for the changes in refractive indices.

AUTHOR INFORMATION

Corresponding Author

*E-mail: ali4@uakron.edu; mohsen.s.yeganeh@exxonmobil.com.

ACKNOWLEDGMENT

We are grateful for the financial support from NSF (CTS-0355304 and DMR-0512156) and ExxonMobil Research and Engineering Co. We also thank Shawn Dougal for technical assistance.

ASSOCIATED CONTENT

Supporting Information. Parameters used in the theoretical fits. This material is available free of charge via the Internet at http://pubs.acs.org.

REFERENCES

(1) Adamson, A. W.; Gast, A. P. *Physical Chemistry of Surface*; Wiley: New York, 1997.
(2) Somarjai, G. A. *Introduction to surface chemistry and catalysis*; Wiley: New York, 1994.
(3) Bain, C. D. *J. Chem. Soc., Faraday Trans.* **1995**, *91*, 1281–1296.
(4) Shen, Y. R. *Proc. Natl. Acad. Sci. U. S. A.* **1996**, *93*, 12104–12111.
(5) Eisenthal, K. B. *Chem. Rev.* **1996**, *106*, 2693–2724.
(6) Richmond, G. L. *Chem. Rev.* **2002**, *106* (8), 2693–2724.
(7) Buck, M.; Himmelhaus, M. *J. Vac. Sci. Technol. A* **2001**, *19*, 2717–2736.
(8) Arnolds, H.; Bonn, M. *Surf. Sci. Rep.* **2010**, *65*, 45–66.
(9) Chen, Z.; Shen, Y. R.; Somorjai, A. G. *Annu. Rev. Phys. Chem.* **2002**, *53*, 437–465.
(10) Shen, Y. R. *The Principles of Nonlinear Optics*; John Wiley & Sons, Inc.: New York, 1984.
(11) Gautam, K. S.; Schwab, A. D.; Dhinojwala, A.; Zhang, D.; Dougal, S. M.; Yeganeh, M. S. *Phys. Rev. Lett.* **2000**, *85*, 3854–3857.
(12) Rangwalla, H.; Schwab, A. D.; Yurdumakan, B.; Yablon, D. G.; Yeganeh, M. S.; Dhinojwala, A. *Langmuir* **2005**, *20*, 8625–8633.
(13) Yang, C.; Wilson, S.-C.; Richter, L. J. *Macromolecules* **2004**, *37*, 7742–7746.
(14) Li, G.; Dhinojwala, A.; Yeganeh, M. S. *J. Phys. Chem. B* **2009**, *113* (9), 2739–2747.
(15) Chen, X. Y.; Wang, J.; Chen, Z. *Langmuir* **2004**, *20* (23), 10186–10193.
(16) Li, G.; Ye, S.; Morita, S.; Nishida, T.; Osawa, M. *J. Am. Chem. Soc.* **2004**, *126* (39), 12198–12199.
(17) Harp, G. P.; Gautam, K. S.; Dhinojwala, A. *J. Am. Chem. Soc.* **2002**, *124*, 7908–7909.
(18) Chen, X. Y.; Wang, J.; Even, M. A.; Chen, Z. *Macromolecules* **2002**, *35* (21), 8093–8097.
(19) Ye, S.; Morita, S.; Li, G.; Noda, H.; Tanaka, M.; Uosaki, K.; Osawa, M. *Macromolecules* **2003**, *36* (15), 5694–5703.
(20) Wilson, P. T.; Briggman, K. A.; Wallace, J. C.; Stephenson, W. E.; Richter, L. *Appl. Phys. Lett.* **2002**, *80*, 3854–3857.
(21) Harp, G. P.; Rangwalla, H.; Yeganeh, M. S.; Dhinojwala, A. *J. Am. Chem. Soc.* **2003**, *125*, 11283–11290.
(22) Lu, N.; Shephard, X. L.; Han, J. L.; Xue, J.; Chen, Z. *Macromolecules* **2008**, *41* (22), 8770–8777.
(23) McGall, S. J.; Davies, P. B.; Neivandt, D. J. *J. Phys. Chem. B* **2004**, *108* (41), 16030–16039.
(24) Tong, Y.; Zhao, Y.; Li, N.; Osawa, M.; Davies, P. B.; Ye, S. *J. Chem. Phys.* **2010**, *133*, 034704.
(25) Tong, Y.; Zhao, Y.; Li, N.; Ma, Y.; Osawa, M.; Davies, P. B.; Ye, S. *J. Chem. Phys.* **2010**, *133*, 034705.
(26) Yeganeh, M. S.; Dougal, S. M.; Polizzotti, R. S.; Rabinowitz, P. *Thin Solid Films* **1995**, *270*, 226–229.
(27) Hirose, C.; Akamatsu, N.; Domen, K. *J. Chem. Phys.* **1992**, *96*, 997–1004.
(28) Yeganeh, M. S.; Dougal, S. M.; Sibernagel, B. G. *Langmuir* **2006**, *22* (2), 637–641.
(29) Harp, H.; Rangwalla, G. P.; Li, G.; Yeganeh, M. S.; Dhinojwala, A. *Macromolecules* **2006**, *39* (22), 7464–7466.